Effect of Processing and Nano scale Reinforcement on the cold forming of Al-TiC Composites

M.Sivaraj[1]*, S.Muthuraman[2], N. Selvakumar[3]

[1]**School of Mechanical and Electro Mechanical Engineering, Hawasaa University, Hawasaa Ethopia,**
[2]**Department of Mechanical Engineering, Higher college of Technology, Muscat, Oman,**
[3]**Department of Mechanical Engineering, MepcoSchlenk Engineering College, Virudhunagar - 626 005, Tamilnadu, India**

Abstract: An investigation on mechanism of deformation and densification behaviour of the Aluminium (Al)-Titanium carbide (TiC) Nanocomposite has been taken out by cold upsetting. Current work has been carried out on the workability behavior of Al composite reinforced with TiC (5% with particle size below 200 *nm*) under Uni-axial stress state conditions. The Al-TiC composite was produced using high energy planetary ball milling. Cylindrical preforms along with initial theoretical density of 85% possessing three different aspect ratios (0.5, 0.75 and 1.0) were prepared using a die and punch assembly with a 100 *tones* capacity Compression Testing Machine. The preforms were sintered in an electric muffle furnace at 575°*C*, and subsequently furnace cooled. Incremental deformation steps were used for conducting the Cold deformation experiments. Lower aspect ratio exhibit enhanced densification and load-bearing capacity compared to that of higher aspect ratio performs. Density become uniform and quite easily due to rapid load transfer resulting in an extensive work-hardening. An attempt is also made to establish relationships between various parameters such as stress & strain and is evaluated.
Key words : Aluminium, Plastic Behaviour, Preform, Characterization, Density, SEM, XRD.

Introduction

Composites have been considered as an important engineering material for potential applications in various industries from the days of their inception. During the last several decades, extensive research has shown tremendous promise of metal matrix composites (MMCs) and a large number of conventional and innovative fabrication techniques have been developed to engineer composites for a diverse field of applications [1-4]. The most common choices for the matrix of a metal matrix composite have been aluminium, magnesium and titanium. The titanium matrix composites were engineered for a spectrum of performance-critical and high temperature related applications. The aluminium alloy-based MMCs were favorable on account of their low density, wide alloying range, capability and response to heat treatment using the existing infrastructure that is used for the monolithic counterparts, and the intrinsic flexibility and responsiveness to both primary and secondary processing. Matrix strengthening by reinforcing nanosized ceramic particles attracts many

 researchers as it maintains good ductility, high temperature creep resistance and fatigue properties [5-8]. The ductility and toughness of such MMCs can be significantly improved with simultaneous increase in strength by reducing the particle size to the nanometer range in the so-called Metal Matrix Nanocomposites (MMNCs) [9]. High-energy mechanical ball milling can be used to produce nano (*nm*) powders from micron (*μm*) size [10-12].

Nowadays, several secondary processing techniques have been used to increase the reduced mechanical properties of PM components due to the presence of residual porosity left after sintering. Precision cold forming can result in higher production of parts with good dimensional control and good surface finish [13]. It is often possible to use cheaper materials with low alloy content because of extensive strain hardening during cold forming. It is also reported [14]. Workability refers to the relative ease with which a material can be shaped through plastic deformation and it is a function of the material as well as the process [15]. To understand the workability criteria of any material, a clear concept on fracture criterion for ductile fracture must be established. The concept of deformation and fracture of powder metallurgy preform still requires a considerable amount of investigation. A number of researchers have reported the experimental and analytical research works on workability of cylindrical preforms. Abdel-Rahman and El-sheikh [16] studied the workability and the effect of the relative density on the forming limit of powder metallurgy (P/M) compacts by conducting upsetting test. A workability factor was presented for the case of uniaxial stress state condition which describes the effect of the mean and the effective stresses. Selvakumar and Narayanasamy [17] have proposed that lower aspect ratio preforms give uniform density and this is due to rapid aspect ratio preforms give uniform density and this is due to rapid load transfer resulting in expensive work hardening. However it is not true for the higher aspect ratio preforms. In metal forming operations, formability of a material is critical technological concept that mainly depends on the ductility of the material and associated process parameters. Several authors [18] investigated workability and/or effects of process parameters on the workability of PM aluminium and/or aluminium metal composites. Narayanasamy et al. [19] formulated an empirical relationship between the formability stress index and the axial strain and also empirical constants were established for relationship between the above said parameters. Hashmi [20] analyzed the dynamic compression of cylinders between flat platens having unequal frictional properties. The velocity field can be used conveniently for the prediction of forging in upset forging of cylindrical billets with dissimilar frictional conditions as the die- material interface [21]. A method of evaluating the effectiveness of various lubricants by measuring the coefficient of friction between metal powder and die wall was developed by Tabata [22]. Narayanasamy and Pandey analyzed the total work hardening in P/M preforms is due to densification as well as cold working of the base material surroundings the pore.

In this paper, a complete investigation on the workability criteria of Al-5% TiC powder preforms were made during cold upsetting. Powder metallurgy preforms with nano particle size and various aspect ratios were discussed for studying the behaviour of workability during cold upsetting under Uni-axial stress state condition. So far, there is no nano size conversion and workability process was carried out in TiC particle reinforced in Al. But in the present work, TiC particle reinforced in Al is converted to nano particle size and workability process was considered. Lesser the particle size of the reinforcement, the mechanical properties will be superior but it is superior only upto 10% of TiC present in the Al. The hardness value is getting reduced above 10%, [23& 24].

Table 1 Characteristics of powder

(a) Characteristics of aluminium powder

	Sieve size (*μm*)	Wt.%
Aluminium	+106	00.26
	+90	02.54
	+75	14.73
	+63	17.58
	+53	24.86
	+45	12.33
	+38	06.27
	-38	21.42
Apparent density (*g. cm^{-3}*)		1.030
Flow rate, (by Hall flow meter) (50*g^{-1}*)		32.00
Particle size-dry sieve test standard		ASTMB-214

Experimental

Materials and its characteristics

Aluminium and Titanium Carbide powders, utilized in the current research, were procured from M/s. Metal powder company (P) Ltd, Tirumangalam, Madurai, Tamilnadu, India and M/s. Alfa Aesar, England. Atomized aluminium powder and TiC were acquired with 99% and 99.5% purity with $45\mu m$ and $2\mu m$ average particle sizes respectively. The characteristics of the aluminium and TiC powder are listed in Table 1(a-b). The TiC powder was pulverized in a planetary ball mill for 12 *h* and the acquired particle size was very nearly below 200*nm*. The individual powders (Al, TiC) were fine-grained in a planetary ball mill using tungsten carbide grinding medium with Ball Powder Ratio(BPR) ratio 1:20for further 1.5 *h* and later it was blended on a mass basis with 5% titanium carbide. Then the combined Al-5TiC powders were mixed systematically in the high energy ball mill for another 0.25 *h* to attain homogeneous mixture. Figure 1(a) shows the initial aluminium particles at 800X magnification; the particles are spherical in structure. Figure 1(b) shows the TiC particles at 1000X magnification and it has the structure of a pancake. Further Figure 1(c) shows Al-5TiC mixed powder after milling for 0.25 *h.*
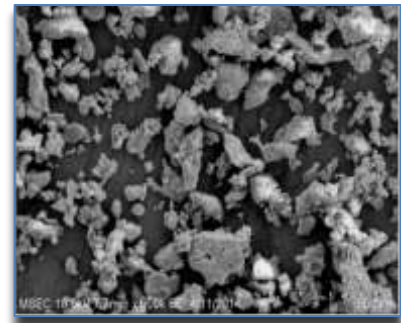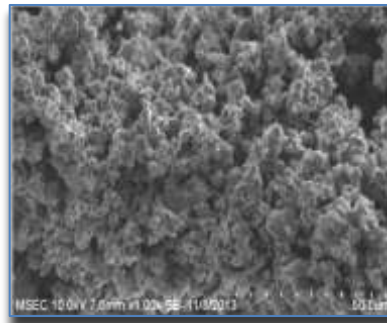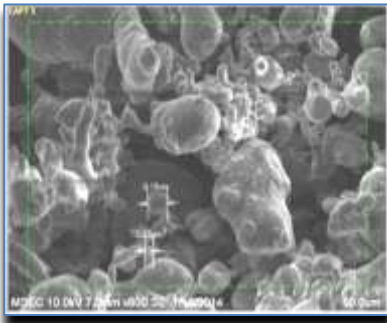
(a) pure Al   (b) pure TiC   (c) Al-5TiC mixed powder
**Fig. 1(a-c) SEM Morphology.**

Compacting

Powder mix matching to Al-5TiC was synthesized on a ball mill to attain a homogeneous powder synthesize. The size of TiC assorted was below 200*nm*.The cold compacts of percent of composite particle ad-combined prime powder were processed by shaping use of high carbon die steel set. Zinc-stearate was pre-owned as lubricant and utilized on the inner surface of the die, outer surface of the punch and the top surface of the butt so as to avoid adhering of powder to these surfaces. A known weight of powder was involved and poured into the die with its butt inserted at the bottom and then the punch was introduced from the top of the die. Green compacts of the powder synthesize was processed on a 1.0×10^6 *N* capacity Compression Testing Machine using suitable punch and die assembly as shown in Figure 2. Cylindrical compacts of 15*mm* diameter with an aspect ratio of 0.5, 0.75 and 1.0 were processed. Compacting pressure was utilized moderately and it was 6.7x107*N/mm²*for three aspect ratios. When preparing the compacts, the initial density and aspect ratio were managed by accurately controlling the mass and accurately monitoring the compacting pressure engaged.

Fig. 2 Compaction methodology.

After compaction, ejection of the compact was done by withdrawing the butt and placing the die on two parallel blocks of same height take off the hole right in the centre of the free space between the two blocks and then applying pressure by means of Compression Testing Machine. The damage of the compacts was avoided by means of supporting cotton under the compact. Thus when the punch starts moving down through the die cavity, the compact comes down in between the space sustained by arranging the supporting blocks. The ejection load of the lower order recommend that there was very little adhering of the powder with the die and the punch surfaces. The flow chart illustrates the various stages of preparation of composites as shown in Figure 3.
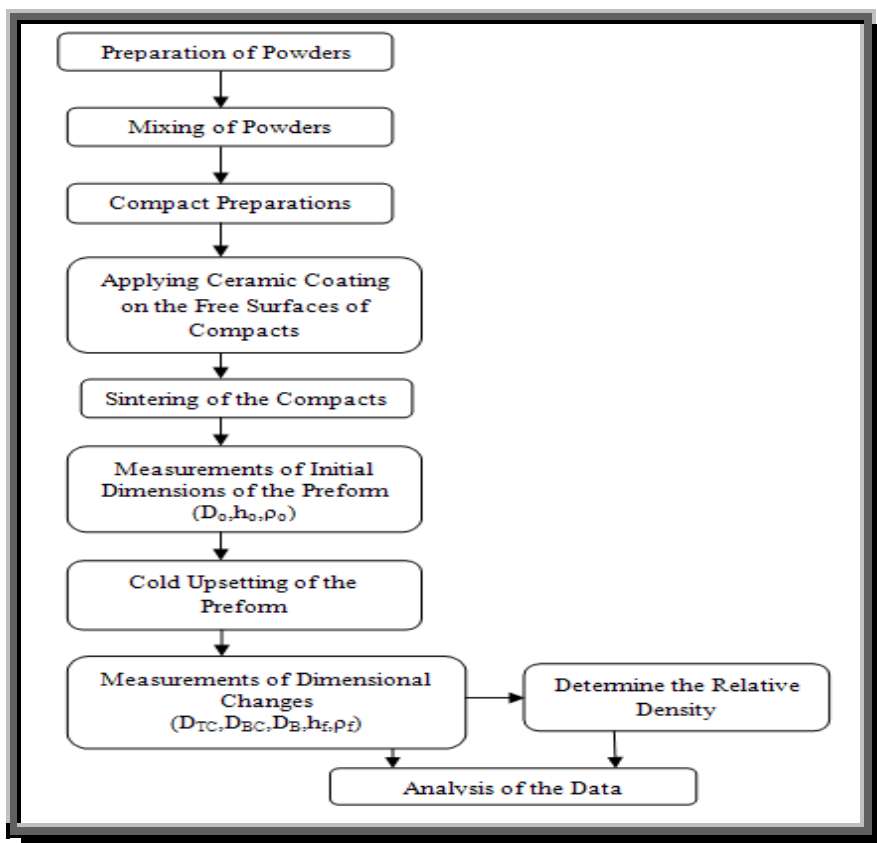
Fig. 3 Flow chart- upsetting of composite.

Sintering

Sintering of powder sequentially involves in the establishment and growth of bonds between the particles of powder at their areas of contact and migration of the grain boundaries formed at the bonds. Bonds formed between the particles during sintering and the number of particles bonds increase as the temperature increases.

The compacts were sintered in an electric muffle furnace in the temperature range of $575°C$ for a sintering time of 60 *min* and allowed to get cooled to room temperature in the furnace itself.After the achievement of sintering, the preforms were clear up by utilizing a fine wire brush.

Cold Deformation

Initial diameter (D_O), initial height (h_O) and the initial preform relative density (ρ_O) of the specimen were measured and noted.Each compact was managed to the incremental compressive loads of 0.005*MN and* the upsetting was carried between two flats, mirror finished open dies on a compression testing machine of $1.0x10^6 N$ capacity. Zinc-sterate was well utilized as lubricant on the ends of preforms and contacting surfaces of flat dies, which make a position for almost frictionless ideal deformation. The deformation was carried out prior to the appearance of first visible crack was observed on the free surface. After each interval of loading, dimensional changes in the specimen such as height after deformation (D_{BC}), bulged diameter (D_B) and density of the preform (ρ_f) were measured. The illustrative diagram showing the various parameters measured before and after deformation is accommodated in Figure 4a and b.

Using the Archimedes principle, the density of upset preforms was also resolved after every loading interval. The deformation tests were continued prior to the fracture developed at outer surface of the specimen as shown in Figure 5. Experimental measurements were also pre-owned to calculate the many parameters namely the stresses, the Poisson's ratio, density ratio and the strain. The Theoretical process to calculate the above parameters are explained in detail under.
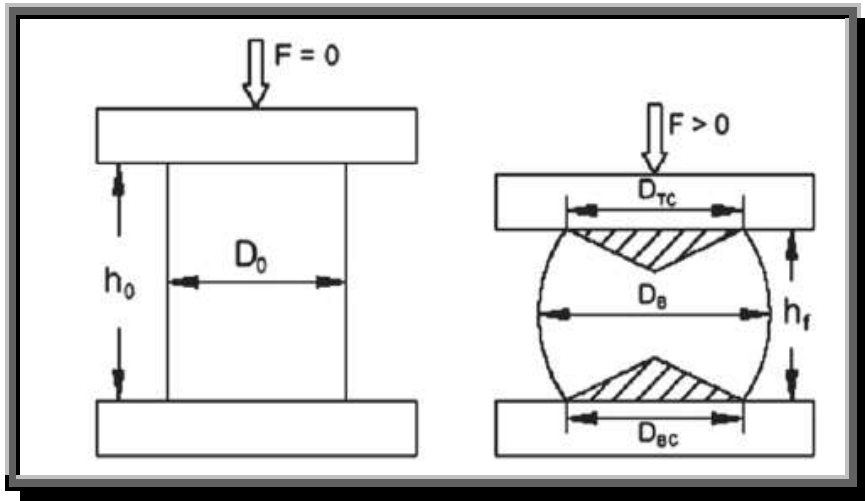

Fig. 4a Upset test preform before and after deformation.

Fig. 4b Upset test preform before deformation.

Fig. 5 Photographs showing upset test preform of after deformation test.

Theoretical Analysis

The modern research is based on the analytical constancy of the deformed density, the stresses and the strains. In this analysis, the composite material under discussion is porous. As related [25, 26] the expression for the fractional density ratio being

$$\left(\frac{\rho_f}{\rho_{th}}\right) = \left(\frac{\rho_o}{\rho_{th}}\right) e^{(\varepsilon_z - \varepsilon_\theta)} \qquad (1)$$

Axial strain $\varepsilon_z = \ln\left(\frac{h_o}{h_f}\right)$ and the hoop strain based on contact and bulged diameters can be

$$\varepsilon_\theta = \ln\left(\frac{[2D_B^2 + D_C^2]}{3D_O^2}\right) \quad (2)$$

Where D_O is the initial diameter of the preform before deformation, D_C is the contact diameter of the preform after deformation, D_B is the bulged diameter of the preform after deformation, h_o is the initial height of the preform before deformation, h_f is the height of the preform after deformation, and ρ_{th} is the theoretical density of the fully dense material.

As the ratio $\left(\frac{\rho_o}{\rho_{th}}\right)$ is taken as constant, Eq. (1) shows the relationship between the density ratios $\left(\frac{\rho_f}{\rho_{th}}\right)$ and the exponential power of the difference between two true strains ε_z and ε_θ.

In addition, the conventional hoop strain (ε_θ') can be calculated as follows:

$$\varepsilon_\theta' = \ln\left(\frac{D_C}{D_O}\right) \quad (3)$$

The new or instantaneous Poisson's ratio (ψ) based on the contact and bulged diameters are as given below:

$$\varphi = \frac{\epsilon_\theta}{2\epsilon_z} \qquad (4)$$

Now the hoop stress based on bulged and contact diameter (σθ) can be derived as interpreted in Ref. [25];

$$\sigma_\theta = (\frac{\alpha+\gamma}{1+\alpha\gamma})\sigma_z \qquad (5)$$

Where $\alpha = (d\varepsilon_\theta/d\epsilon_z)$ and the conventional Poisson's ratio (γ) is given below:

$$\gamma = \frac{\varepsilon'_\theta}{\varepsilon_z} \qquad (6)$$

Now substituting the value for the true axial stress σz,the true hoop stress σθ , can be calculated from Eq. (5), where

$$\sigma_z = \frac{Load}{Contact\ surface\ area}$$

In addition, using the values of σz and σθ, the hydrostatic stress (σm) can be calculated using the relationship given below:

$$\sigma_m = \frac{1}{3}(\sigma_\theta + \sigma_z) \qquad (7)$$

Results and discussion

Effect of X-ray diffraction

The specimen reinforced with 5%TiC has X-ray diffraction (XRD) patterns and is shown in Figure 6. After sintering of compacts, this test was conducted. Aluminiumand TiC peaks were indexed using JCPDS files (file no. 04-0787 and 32-1383 respectively). The presence of Aluminium matrix and TiC particles in the composite was confirmed by the XRD pattern. Clearly, a few main peaks are visible in the XRD patterns as shown in Figure 6.3(a). Diffraction patterns which are relative to Al powder exhibits peaks at 39.5^0 , 45.2^0 , 65.3^0 and 79.5^0 respectively to the (111), (200), (220) and (311) reflections of F.C.C. Diffraction patterns which are relative to TiC powder exhibits peaks at 36.5^0 , 42.5^0 , 61.5^0 and 73.5^0 respectively to the (111), (200), (220) and (311). Thepatterns which have the peaks gave a good match with the references patterns (JCPDS) [28].
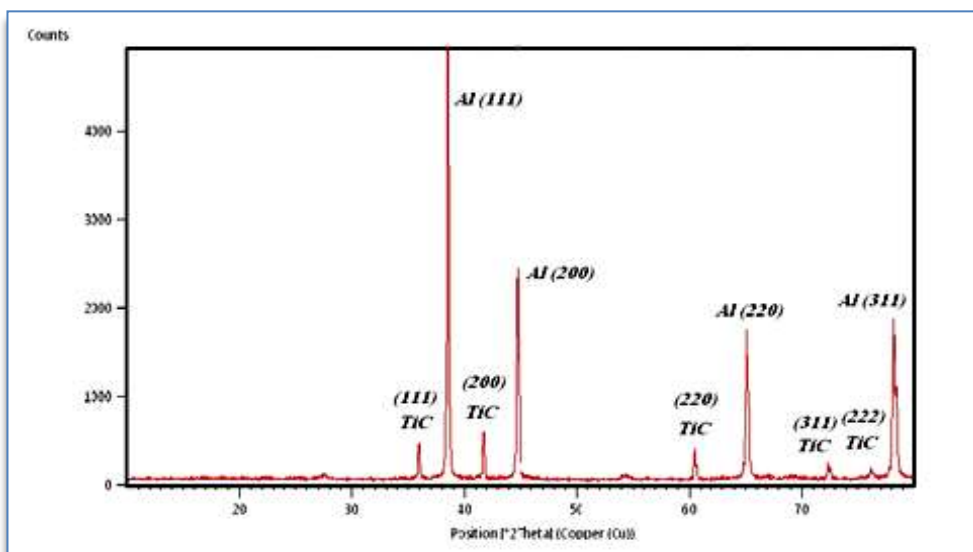

Fig. 6 XRD for Al-5% TiC composite JCPDS file no. 04-0787 and 32-1383.

Effect of microstructural evaluation

Microstructural evaluation studies were conducted by FESEM. The composite specimen showed the uniform distribution of reinforced particles. An observation reveals minimum presence of porosity in the materials [29]. Figure 5 shows the FESEM microstructure of the sintered composite samples of aluminium composites with below 200nm TiC particles respectively. A close observation of the above micrographs indicates the even distribution of TiC particles in the aluminium matrix Al-5TiC ($\leq$200nm) composites.Grey regionshows Al matrix and dark grey and cornered particles shows the reinforcement component of TiC. It is clearly noted that TiC particles are well dispersed and uniformly distributed in Al matrix. The uniform distribution of TiC particles can be attributed to the time and the method of mixing. To enhance the mechanical properties, it is very important to obtain homogeneous reinforcement in the matrix, for the composite materials.
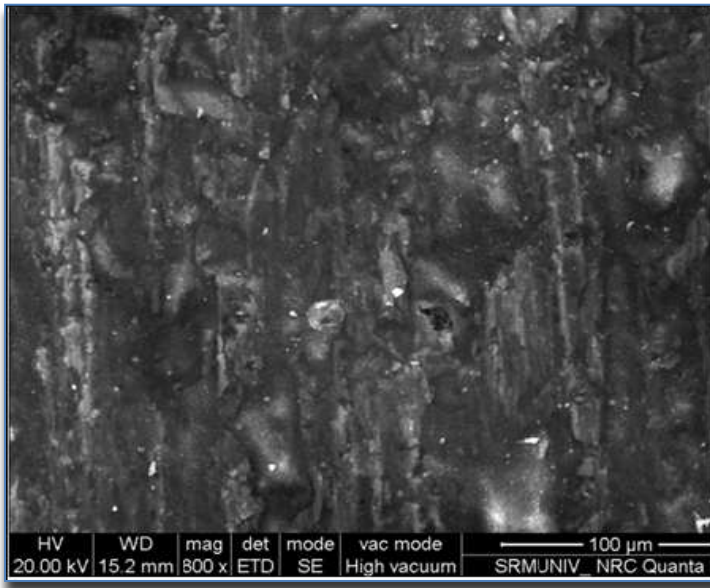

Fig. 7 FESEM of as sintered Al-5%TiC P/M preform.

Effect of deformation Behavior of Preform

The results of deformation behaviour of 85% initial fractional density, Al-5%TiC composite preforms are explained in this section. The following stress strain relationship respecting the plastic deformation is explained in detail for the many aspect ratios with Zinc-sterate lubricants.

Effect of various stresses & axial strain

Using the simple theory of plasticity, the axial stress (σ_z), the hoop stress (σ_θ) and the hydrostatic stress (σ_m) were determined and planed against the axial strain (ε_z) for different aspect ratios in figures 8(a-c) for the Al-5%TiC composite preforms. The hoop stress is tensile in nature because during compressive deformation, the bulged diameter expands due to the action of secondary tensile stress. However, for any deformation level, the increase in the hoop stress due to deformation is appreciably low compared to the axial stress. However, the value of the hydrostatic stress is much less than the other stresses, namely the axial stress (σ_z) and the hoop stress (σ_θ) and it is also compressive in nature, at different strain level. For all preforms, the axial and the hoop stress level also increases for a given aspect ratio. The values of the axial stress, the hoop stress and the hydrostatic stress are high for the lower aspect ratio (0.5) than higher aspects ratios (0.75 and 1.0) preforms. As the axial strain increases the fractional density also increases irrespective of aspect ratio, because pores are getting closed. It has been noticed that for the selected range of aspect ratios and relative densities, the initiation of the crack of the preforms has been noticed at a very high strain value for the cases of the preforms having lower aspect ratios and higher fractional densities, because pores are less.

(a)

(b)

(c)
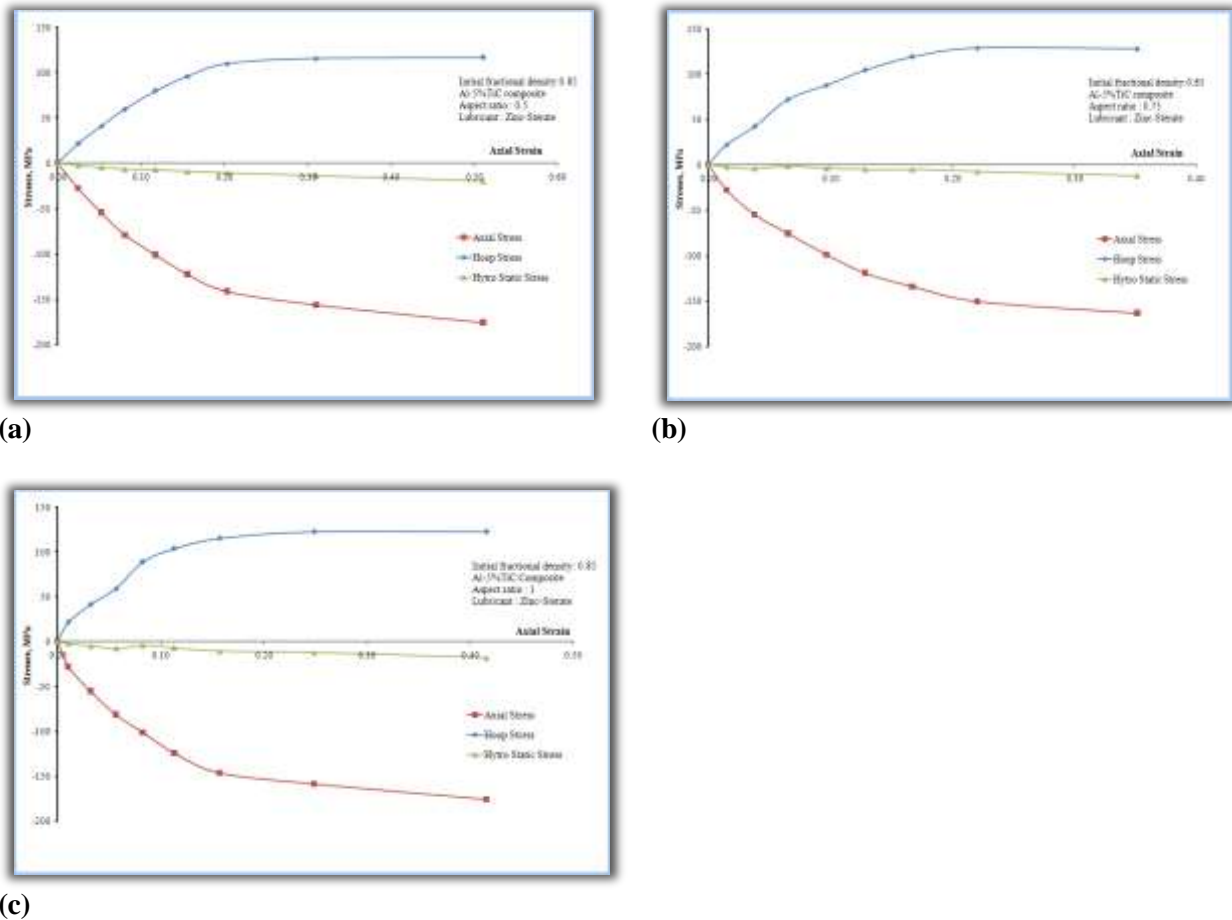
Fig. 8 The variation of stresses with respect to axial strain for various aspect ratios (a) 0.5 (b) 0.75 (c) 1.0.

Effect of axial stress & axial strain

Stress-strain analysis is examined to be the fundamental when discussing the mechanical behaviour of any wrought or P/M materials subjected to any form of loading condition [29]. Stress finds the internal resistance of a material against the external disturbance on a particular area of cross section exposed to deformation while strain normally deals with the deformation of the body. Figure 9 shows the effect of with 5%TiC in Al on the characteristic features of the axial stress, σ_z, as a function of the axial strain, ε_z, for three different aspect ratios. It is noticed that effect of TiC in Al is quite dominant in the later stages than in the initial stages of deformation, this being true invariable for all aspect ratios. It shows that the true axial stress increases rapidly as the true height strain is increased, followed by a gradual increase in true axial stress with further increase in true height strain. Further, it is found that a preform with higher aspect ratio exhibits improved load bearing capacity compared with the lower aspect ratio, subject to the condition that the initial preform density and deforming media taken is kept constant. As a TiC particle increases the porosity level decreases and the relative density increases for the high aspect ratio. This may be one of the reasons for the increasing stresses for higher aspect ratio and also the stress parameter also increases because the true hoop stress (σ_θ) continues to increase rapidly during deformation.
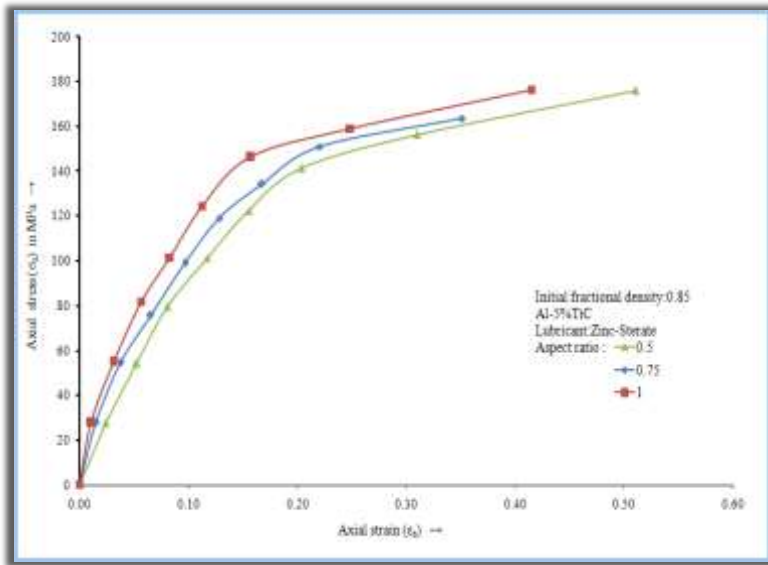
Fig. 9 The relationship between σ$_z$ and ε$_z$.

Effect of fractional density & strain parameter

Figure 10 has been drawn to establish the relationship between the fractional density and the exponential of $e^{(\varepsilon_z - \varepsilon_\theta)}$ in accordance with the derived relationship of [30] provided in the theoretical discussion. These plots correspond to three initial aspect ratios, namely, 0.5, 0.75 and 1.0, all possessing same initial preform density. These plots established a straight-line relationship between the fractional density$(\frac{\rho_f}{\rho_{th}})$ and the exponential of $e^{(\varepsilon_z - \varepsilon_\theta)}$ with different slopes. The rate of change of densification parameter with respect to the exponential of $e^{(\varepsilon_z - \varepsilon_\theta)}$ is very much greater for lower aspect ratio when comparing with higher aspect ratio because it has lesser porosity. The TiC particle occupies the pores between Al particles. Since the pore size is very small, densification value increases during plastic deformation. It is further observed that the pore size becomes smaller and smaller for the lower sizes of TiC content and hence the densification value also increases. As the aspect ratio increases the densification decreases because of more porous bed height. This indicates that the aspect ratio value 0.5 (smaller value) shows better densification compared to other aspect ratio.
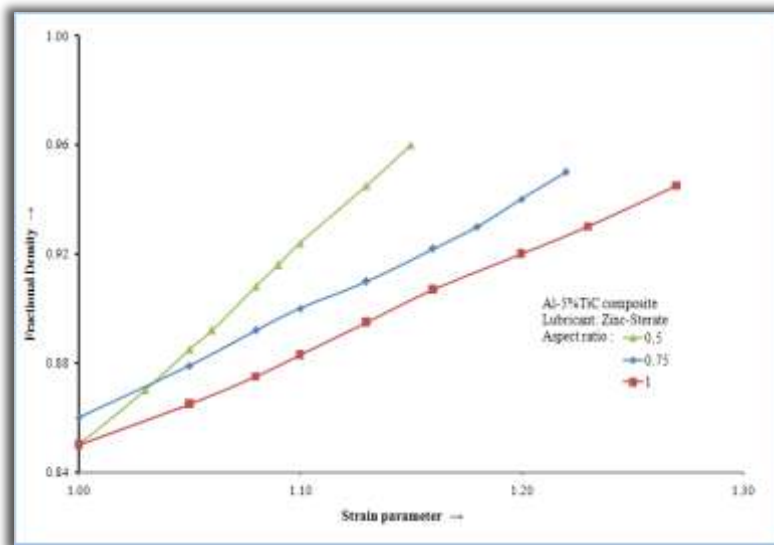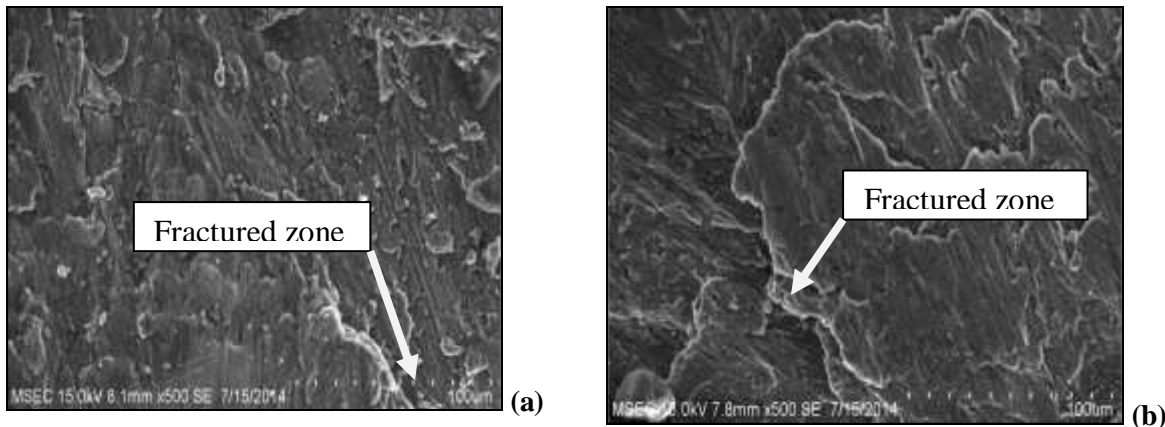

Fig. 10 The relationship between fractional density and strain parameter.

Fig. 11 The SEM images of fracture of Al-5TiC sintered preforms after upsetting (a) Aspect ratio 0.75 (b) Aspect ratio 0.5.

Effect of fractography analysis

Figure 11(a-b) shows the fracture details of Al-5TiC with aspect ratio of 0.75 and 0.5 at 500X magnification respectively. Assoon as the composite is ductile in nature, the fracture also tends to act like the same, and the fracture boundaries are clearly observable in above figures. And also the above said microstructure illustrates the joining of pores & the formation of cracks through upset forming operation. It is further scrutinized that as the initial preform density increases due to aspect ratio (0.5), the crack width on the outer surface of preforms also decreases which shows fine cracks. This indicates that the cracking tendency is postponed for the case of low aspect ratio.

Conclusions

The following conclusions can be drawn from the above results and discussions.

- An exponential relationship is established between the fractional theoretical density $(\frac{\rho_f}{\rho_{th}})$ and $e^{(\varepsilon_z - \varepsilon_\theta)}$. This relationship is valid for all the aspect ratios.
- The axial stress has an increases trend with higher level of deformation till failure. This is because, at the time of raising the load, the apertures in the preforms are flattened and contact surfaces are increased. Hence, the load- bearing capacity increases steeply through increase of strain.
- Lower aspect ratio exhibits improved densification and load-bearing capacity compared to so as to of higher aspect ratio performs density uniformly and quite easily by reason of rapid load transfer resulting in extensive work-hardening.
- The fractional density decreases in the higher aspect ratio.

References

1. Torralba, J.M.; Da Costa, C.E.; Velasco, F; P/M aluminium matrix composites: an overview. J Mater Process Technol., 2003, 133, 203-206.
2. Abouelmagd, G.; Abd, El-Mageed, A. M; Proceedings of the 5th International Conference on Measurement and Control of Granular materials. XI AN China., 2000, 69-76.
3. Tokaji, K.; Shiota, H.; Kobayashi, K.; Effect of particle size on fatigue behaviour in SiC particulate-reinforced aluminium alloy composites. Fatigue FractEng Mater Struct., 1999, 22, 281-288.
4. Zhu, S.J.; Peng, L.M.; Zhou, Q.; Ma, Z.Y.; Kucharova, K.; Cadek, J; Creep behaviour of aluminium strengthened by fine aluminium particles and reinforced by silicon carbide particulates DS Al-SiC/Al4C3 composites. Mater Sci Eng. A., 1999, 268, 236-245.
5. Hassan, S.F.; Gupta, M; Development of high strength magnesium copper based hybrid composites with enhanced tensile properties. Mater Sci Technol., 2003, 19, 253-259.

6.   Hassan, S.F.; Gupta, M; Development of high strength magnesium copper based hybrid composites with enhanced tensile properties. Composite Structures., 2006, 72, 19-26.

7.   Laha, T.; Chen, Y.; Lahiri, D.; Agarwal, A; Tensile properties of carbon nanotubes reinforced aluminiumnanocomposites fabricated by plasma spray forming. Compos. A., 2009, 40, 589-594.

8.   Santos-Beltran, A.; Gallegos-Orozco, V.; Goytia, Reyes, R.; Miki-Yoshida, M.; Estrada-Guel, I.; Martinez-Sanchez, R; Mechanical and microstructural characterization of dispersion strengthened Al-C system nanocomposites. J. Alloys Compd., 2010, 489, 626-630.

9.   Montealegre, Melendez, I.; Neubauer, E.; Angerer, P.; Danninger, H.; Torralba, J.M; Influence of Nano-Reinforcements on the Mechanical Properties and Microstructure of Titanium Matrix Composites. Composites Science and Technology., 2011.

10.   Vettivel, S. C.; Selvakumar, N.; Narayanasamy, R.; Leema, N; Numerical modeling, prediction of Cu–W nano powder composite in dry sliding wear condition using response surface methodology. Mater Des., 2013, 50, 977-996.

11.   Mordike, B.L.; Kaczmr, J.; Kielbinski, K.U; Effect of tungsten content on the properties and structure of cold extruded Cu-W composite materials. Powder MetallInt .,1991, 23, 91-96.

12.   Senthil, Kumar, V.; Balaji, A.; Hafeez, Ahamed; Effect of secondary processing and Nanoscale reinforcement on the mechanical properties of Al-TiC composites. Journal of minerals and Materials Characterization and Engineering., 2011, 10, 1293-1306.

13.   Narayan, S.; Rajeshkannan, A; Densification behaviour in forming of sintered iron-0.35% carbon powder metallurgy preform during cold upsetting. Mater Des., 2011, 32, 1006–13.

14.   Bensam, Raj, J.; Marimuthu, P.; Prabhakar, M.; Anandakrishnan, V.; Effects of sintering temperature and time intervals on workability behaviour of Al–SiC matrix P/M composite. J AdvManuf Technol., 2012, 61, 237–52.

15.   Dieter, George; Hand book on workability analysis and applications. 1st ed.USA, ASM Publications., 2002.

16.   Abdel-Rahman, M.; El-Sheikh, M.N; Workability in forging of powder metallurgy compacts, J Mater Process Technol., 1995, 54, 97-102.

17.   Selvakumar, N.; Narayanasamy, R; Phenomenon of strain hardening behaviour of sintered aluminium preforms during cold axial forming, J Mater Process Technol., 2003, 142, 347-54.

18.   Zhang, X.Q.; Peng, Y.H.; Li, M.Q.; Wu, S.C.; Ruan X.Y; Study of workability limits of porous materials under different upsetting conditions by compressible rigid plastic finite element method. J Mater Process Eng 2000, 9, 164–9.

19.   Narayanasamy, R.; Ponalagusamy.; Subramanian, K. R; Generalized yield criteria of porous sintered powder metallurgy metals. J Mater Process Technol., 2001, 110, 182-185.

20.   Hashmi, M.S.J; Upsetting of cylindrical billets between flat platens having unequal frictional properties. Int J Mach Tool Des. 1978, 18, 189-196.

21.   Mohan Raj, A.P.; Selvakumar, N.; Narayanasamy, R.; Kailasanathan C; Experimental investigation on workability and strain hardening behaviour of Fe–C–Mn Sintered composites with different percentage of carbon and manganese content. Mater Des., 2013, 49, 791–801.

22.   Tabata, T.; Masaki, S; Coefficient of friction between metal powder and wall during compaction. Powder Metall., 1982, 13, 179.

23.   Sivaraj, M.; Selvakumar, N; Experimental Analysis of Al-TiC Sintered Nano Composite on EDM Process Parameters Using ANOVA. Mater. Manuf. Process., 2016, 31, 801-812.

24.   SeropeKalpakjian.; Steven R. Schmid; Manufacturing Engineering and Technology; Pearson: India, 2015.

25.   Narayanasamy, R.;   Pandey, K.S; Salient features in the cold upset forming of Aluminum-3.5% Alumina powder composite preforms. J Mater Process Technol., 1997, 72, 201-207.

26.   Narayanasamy, R.; Pandey, K. S; Phenomenon of barreling in Aluminum solid cylinders during cold upset forming. J Mater Process Technol., 1997, 70, 17-21.

27.   Williamson, K.; Hall, W. H; X-ray line broadening from aluminium and wolfram. ActaMetallurgica., 1953, 1, 22-31.

28.   Santosh, Kumar.; Prosenjit, Das.; Sandeep, K.; Tiwari, Manas, K.; Mondal, Supriya, Bera.; Himadri, Roy.; Sudip, K.; Samantha; Study of microstructure evolution during semi-solid processing of an In-situ Al alloy composite. Mater Manuf Process., 2015, 0, 1-11. doi:10.1080/10426914.2014.952040.

29.   Rajeshkannan, A.; Narayanan, S; Strain hardening behaviour in sintered Fe-0.8%C-1.0%Si-0.8%Cu powder metallurgy preform during cold upsetting. J Eng Manuf., 2009, 23, 1567-74.

30.   Selvakumar, N.; Narayanasamy, R; Deformation Behavior of Cold Upset Forming of Sintered A1-Fe
       Composite Preforms. J Eng Mater Technol., 2005, 127,241-246.

*****